

Simulating photo-dissociation in strong field by the random phase thermal wavefunction approach

Bar Ezra¹, Ronnie Kosloff¹, and Shimshon Kallush^{1,2}

¹The Institute of Chemistry and the Fritz Haber Centre for Theoretical Chemistry,
The Hebrew University of Jerusalem

²Sciences Department, Holon Academic Institute of Technology, 52 Golomb Street,
Holon 58102, Israel

Abstract

Simulating photo-dissociation processes is a challenging task when the number of states involved is significantly large. We present an ab-initio quantum model for strong field photo-dissociation processes which incorporates rotational dynamics. The computational complexity was reduced by employing the random phase thermal wavefunction method. The simulation outcome are analogous to experimental observable, such as the momentum angular distribution of the photo-fragments. We studied the convergence of these observables at two field intensities. The simulation method can be applied to wide-ranging time-domain spectroscopy at experimental conditions far beyond the reach of accurate direct numerical methods.

1 Introduction

Time domain spectroscopy can be directly modeled by solving the time-dependent Schrödinger equation. Direct modeling for strong field photo-dissociation has almost no alternative. Analytical methods do not apply and perturbation expansions do not converge. This work presents an ab-initio simulation method applicable to the photo-dissociation process of a diatomic molecule. The simulation is guided by strong field pulsed experiments. The goal is that the outcome of the simulation could be directly comparable to experimental observables, explicitly to the velocity distribution of the photo-fragments. We define an ab initio simulation to be free of empirical parameters: based on the Hamiltonian, initial temperature, charge, and mass.

The knowledge of the total Hamiltonian and initial state is required to solve the time-dependent Schrödinger equation. The Born–Oppenheimer approximation allows to separate the electronic and the nuclear terms[1]. Ab initio electronic structure methods are able to accurately calculation the electronic potential surfaces and the transition dipole moments associated with the photo-dissociation [2, 3]. The present study concentrates on solving the nuclear dynamics, specifically dynamics of the vibration and rotation degree of freedom of a diatomic molecule. The radiation field couples electronic vibration and rotation degrees of freedom of the molecule. As a results this strong coupling opens channels to the unbound electronic state where the molecule dissociate.

In the specific experiment we want to simulate[4, 5], the photo-fragments are observed far from the dissociation point. The simulation should be able to calculate the same observable specifically the angular distribution of the outgoing momentum. Such a calculation is set in a large phase-space volume, which translates to a very large computation Hilbert space. In the weak field regime, when one can use perturbation theory the calculation is simplified significantly since selection rules limit

the accessible Hilbert space. In strong field photo-dissociation process many interference channels become open. As a results the calculation has to include all the relevant quantum state that participate in the dynamical process.

Solving the time-dependent Schrödinger equation for a large Hilbert space is a difficult task. The computation effort scales with the size of the Hilbert space, the product of the energy range, and time period. The Hilbert space size is determined by the phase-space volume containing the problem. The phase-space is restricted by the maximum energy the molecule can carry and by the asymptotic distance estimated by the effective dissociation point. The number of angular momentum states required for the calculation is determent by the initial temperature of the molecule and the strength of the radiation field. Each participating photon changes the rotational angular momentum by one unit of \hbar . Therefore when the molecule is subject to strong radiation field the manifold of the accessible states increases significantly. For a typical diatomic photo-dissociation study the Hilbert space is vast, of the order 10^6 . In principle the initial state is a mixed state formally requiring a density operator description. The dimension of the density operator is the square of the Hilbert space, this means that such a calculation is prohibitive expensive.

The random phase wavefunction (RPW) method is employed to overcome the challenge of the large Hilbert space. It replaces a density operator calculations by a finite sample of random phase thermal wavefunctions [6]. Previously the method has been used to calculate the dynamic of molecular systems including rotational states [7, 8, 9]. The present study is aimed to develop methods to calculate the full asymptotic photo-fragment distribution. This requires to study the convergence of the calculation with respect to the number of RPW employed. Typically in the RPW theory the convergence of the observables scales with the number of realization, K , and the Hilbert size, N_S , as $\sim \frac{1}{\sqrt{K}} \cdot \frac{1}{\sqrt{N_S}}$ [7]. We want to investigate the prefactor of this scaling, or particularly what is the number K of RPW that is required to converge a specific observable to experimental accuracy. The most difficult observable to converge is the final momentum angular distribution. The probability of a photo-fragment to be realized in specific pixel is extremely small. Such rare events are hard to converge.

The developed simulation is general, it can be used to calculate a variety of processes and systems. We choose to model the F_2^- system. The motivation is the recent experimental study by Strasser *et al.* [4, 5]. The system can be simulated using four electronic potential energy surfaces. Higher energy potentials are 10 eV above the four surfaces considered and can be ignored. For this system accurate ab-initio potentials have been calculated [2]. Therefore if the nuclear dynamical calculation can be converged, the F_2^- system can be simulated from first principles.

2 Physical Model

The dynamics of a gas phase diatomic molecule takes place on n electronic surfaces and three ro-vibrational inter nuclear degrees of freedom. The system Hamiltonian includes the nuclear Hamiltonian of all electronic states, and the radiation coupling elements between the states mediated by the transition dipole moment. In a Born–Oppenheimer expansion [1] the Hamiltonian can be written as:

$$\hat{H}_{\text{sys}} = \sum_n \left(\hat{H}_n \otimes |n\rangle \langle n| + \sum_{k \neq n} \boldsymbol{\mu}_{n,k} \cdot \boldsymbol{\varepsilon} \otimes |n\rangle \langle k| \right) \quad (1)$$

$$\hat{H}_n = \frac{\hat{P}_r^2}{2m_r} + V_n(r) + \frac{1}{2I} \hat{R}^2 \quad (2)$$

where \hat{H}_n is the nuclear Hamiltonian operator of the n 'th electronic state, that compose of the electronic potential of the n electronic state, $V_n(r)$, and the total nuclear kinetic energy. The kinetic energy

composed by the linear motion, $\frac{\hat{p}_r^2}{2m_r}$, and the rotational motion, $\frac{1}{2I}\hat{\mathbf{R}}^2$. Where, $I = 2m_r r^2$ is the moment of inertia, and $\hat{\mathbf{R}}$ is the nuclear rotational angular momentum operator. The laser field, ε , is a pulse with the parameters that present at table 1.

The scalar product between the transition dipole operator, $\mu_{n,k}$, and the radiation field, ε , can generate different transition schemes. The specific scheme is influenced by the states involved, symmetries and the field polarization. The details are elaborated in our previous work [10]. The present study contains only Σ singlet electronic state, therefore, the nuclear rotational angular momentum operator is equal to the total angular momentum of the molecule, $\hat{\mathbf{R}} = \hat{\mathbf{J}}$. In Hund's case (a) [11], the most common case and the one used here, the projection of $\hat{\mathbf{J}}$ on the laboratory axis, \hat{Z} , is m and on the internuclear axis is Ω .

The internuclear degree of freedom of the molecule is defined by the distance between the two atoms, r , and the molecular orientation, represented by the angles θ and φ . Similar to our previous work, we expand the angles coordinate employing the Wigner rotation matrix, $D_{m,\Omega}^j(\varphi, \theta)$ basis set. Working with this basis set, each state is described by the values of r, j, m , and Ω . The density matrix of the molecule state at time t is:

$$\hat{\rho}(r, r', \theta, \theta', \varphi, \varphi', n, n'; t) = \sum_{\zeta, \zeta'} |n\rangle \langle n'| \otimes a_{n,n',\zeta,\zeta'}(r, r'; t) \otimes |\zeta\rangle \langle \zeta'| \quad (3)$$

where the summation is over all rotational states, $\zeta = \{j, m, \omega\}$, thus $|\zeta\rangle$ is the wavefunction with the quantum numbers $|j, m, \Omega\rangle$, that expanded by the $D_{m,\Omega}^j$ matrices. $a_{n,n',\zeta,\zeta'}(r, r'; t)$ is the nuclear matrix coefficients at each electronic and rotational state. Since this work includes only Σ states the value of Ω is fix, and equal to $\Omega = 0$, so that the matrices are equal to the spherical harmonics functions, $Y_{j,m}(\varphi, \theta)$, and the coupling elements between the state, due to the interaction with the external field, are proportional to $D_{0,0}^1 \propto \cos(\theta)$.

To mimic the experimental process a thermal ensemble of molecules is subjected to a pulsed laser source. Within the temperature considered, the electronic and vibrational degrees of freedom are in their ground state. The initial state is a Boltzmann distribution of several rotational components and can be written as:

$$\hat{\rho}(r, r', \theta, \theta', \varphi, \varphi', n, n'; t=0) = \sum_{j_i} P_B(j_i) a_{0,0,\zeta_i,\zeta_i}(r, r'; t=0) \cdot |0\rangle \langle 0| \otimes \hat{P}_{0,j_i}(r) \otimes |\zeta_i\rangle \langle \zeta_i| \quad (4)$$

where $\hat{P}_{0,j_i}(r) = |\Phi_{n=0,j_i}(r)\rangle \langle \Phi_{n=0,j_i}(r)|$ the projection to the ground vibrational state, that conditioned by the rotational state, j_i . $P_B(j_i) = \frac{\exp(-\beta E_{j_i})}{\mathcal{Z}}$, where $\mathcal{Z} = \sum_l (2l+1) \exp(-\beta E_l)$ is the normalized Boltzmann probability coefficients for each rotational state. Note, that the rotational energy eigenvalues, that satisfy $\hat{H}_{rot} |\psi_{\zeta_i}\rangle = E(j_i) |\psi_{\zeta_i}\rangle$, depend only on the total angular momentum j .

The time evolution of the state is carried out by a first principle propagation of the time-dependent Schrödinger equation: $\hat{\rho}(t) = \hat{U}(t) \hat{\rho}(t=0) \hat{U}^\dagger(t)$ where $i\hbar \frac{d}{dt} \hat{U}(t) = \hat{H}(t) \hat{U}(t)$.

Observables are calculated by the data provided by the density operator, $\hat{\rho}(t)$ so that for any operator \hat{A} :

$$\langle \hat{A} \rangle_t = \text{tr}(\hat{A} \hat{\rho}(t)) = \text{tr}(\hat{A} \hat{U}(t) \hat{\rho}(t=0) \hat{U}^\dagger(t)) \quad (5)$$

Under the common experimental conditions for the molecular beam considered here, the typical incoherent processes such as collisions and spontaneous decay take place on the time scales of $t \geq 1 \text{ nsec}$. The dissociation under 30 fsec laser pulse, is achieved by $\sim 100 \text{ fsec}$. The dynamics are therefore coherent. The expectation value can be thus evaluated, employing the basis where the initial density operator is diagonal $|\tilde{\psi}_{0,0,\zeta_i}\rangle = |\psi_0^e\rangle \otimes |\psi_0^v\rangle \otimes |\zeta_i\rangle$, giving by:

$$\langle \hat{A} \rangle_t = \sum_{n,v,\zeta} P_B(j_i) \langle \hat{U}^\dagger(t) \tilde{\psi}_{0,0,\zeta_i}(t=0) | \hat{A} | \hat{U}(t) \tilde{\psi}_{0,0,\zeta_i}(t=0) \rangle \quad (6)$$

Using equation (6) we can decompose the expectation value into the expectation values of the individual components. Each component requires the time-dependent Schrödinger equation solution for a wavefunction: $i\frac{d}{dt}\psi = \hat{H}(t)\psi$. Numerical methods for the wave function propagation such as the Chebychev approximation that scale as N_S^2 [12, 13, 14, 15]. Observables that are computed by equation (6) are numerically converged and will be used as a reference to the results that will be derived by the random phase method.

The size of Hilbert space of linear molecules, that is the number of occupied states N_S , scales linearly with the temperature. The experiments considered on F_2^- is carried out at an estimated temperature of $T = 100K$. At this temperature the Hilbert space size of the full system is $N_S \sim 10^6$, therefore computing the dynamics with an elevated temperature is becoming an extremely challenging task.

The light induced coupling between the states contributes also to the complexity of the problem. At low intensity the transition can be approximated perturbatively which keeps the scale of interacting states to N_S^2 , while at high intensities the process requires full and exact calculation, which increase the scale of the states to N_S^3 .

To overcome the challenge of the large number of the state, the random phase wavefunction method is used. An efficient representation of the state is done by the use of a limited ensemble of pure states mimicking the initial thermal ensemble. The initial state of a single random phase wavefunctions is written as:

$$|\Psi^k(r, \theta, \varphi; t=0)\rangle = \sum_{\zeta_i} e^{i\chi_{\zeta_i}^k} \sqrt{P_B(j_i)} \sqrt{\tilde{a}_{0,\zeta_i}(t=0)} |0\rangle \otimes |\Phi_{0,\zeta_i}(r)\rangle \otimes |\zeta_i\rangle \quad (7)$$

where the phases $\chi_{\zeta_i}^k$ are chosen randomly, and $\tilde{a}_{0,\zeta_i}(t=0)$ are the coefficients corresponding to the diagonal elements of $a_{0,0,\zeta_i,\zeta_i}(r, r; t=0)$. The propagation of the wavefunction is done according to equation 6, $|\Psi^k(r, \theta, \varphi; t)\rangle = U|\Psi^k(r, \theta, \varphi; t=0)\rangle$. For large number of realization k , the set of random phase wavefunctions are complete basis of states:

$$\lim_{K \rightarrow \infty} \sum_{k=1}^K |\Psi^k(r, \theta, \varphi; t)\rangle \langle \Psi^k(r', \theta', \varphi'; t)| = \hat{\rho}(r, r', \theta, \theta', \varphi, \varphi', n, n'; t) \quad (8)$$

The efficiency of the random phase wavefunction method increases with the size of Hilbert space (and the number of random phases) increase, i.e. with increasing temperature. On the other hand, when increasing the laser field intensity, significant interferences of excitation de-excitation pathways take place. Adding a random phase to the initial state influences the dynamics and introduces additional interference. Therefore, increasing the laser intensity reduces the accuracy of observables that are affected by the dynamical interferences.

The time dependent observables are computed for each random phase wavefunction and then averaged over K realization. The error with respect to the exact solution, the reference, decreases with the number of realization, K . The error scales as $\sim K^{-\frac{1}{2}}$ and $\sim N_S^{-\frac{1}{2}}$.

$$\langle \hat{A} \rangle_t^K = \frac{1}{K} \sum_{k=1}^K \sum_{n,v,\zeta} \langle \Psi^k(r, \theta, \varphi; t) | \hat{A} | \Psi^k(r, \theta, \varphi; t) \rangle \quad (9)$$

In the following section, we present the results calculated by using the random phase wavefunction method on the spatially resolved photo-dissociation. The quantum observables are then compare to a numerically exact computations[10].

3 Results

An ab-initio simulation has been designed to simulate the photo-dissociation process of a diatomic molecule. The RPW method has been employed to overcome the large Hilbert space challenge. Thus,

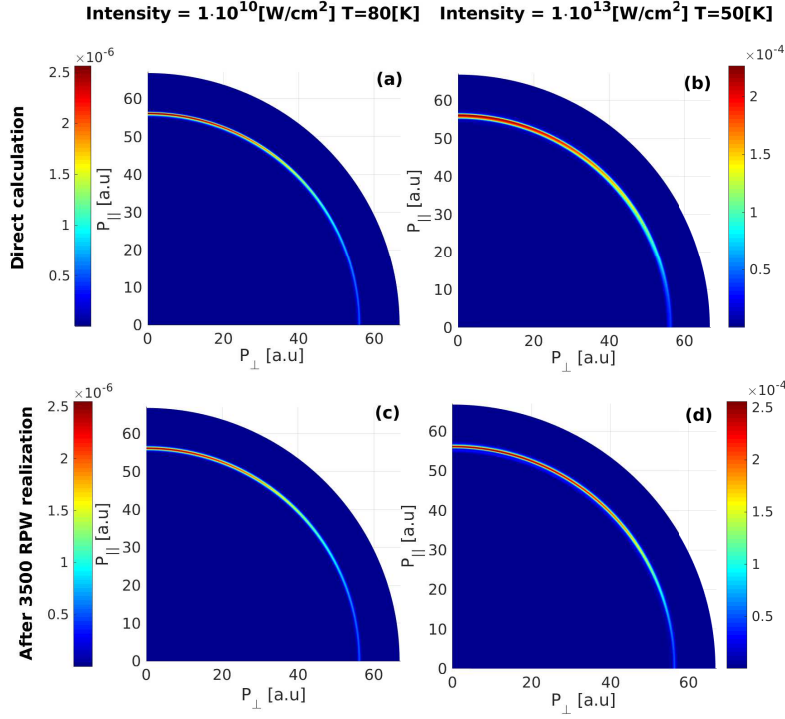


Figure 1: Angular distribution of the outgoing momentum shown as a density plot. Panels a,c show one photon transition process for low laser intensity. Multi-photon transition process, for high laser intensity, are displayed in panel b,d. Upper panels a-b, are obtained by the exact calculation, while the bottom panels c-d, are obtained using the random phase wavefunction method.

the initial state was sampled from the Boltzmann thermal state by random phase wavefunctions, equation (7). The photo-fragments outcome state is represented by the final density operator composed from averaging the individual samples, Eq. (8). The averaged density operator converges to the exact density operator, obtained by simulating the process with the full initial Boltzmann state.

The outcome of the simulation are observables which are directly comparable to the experimental observation. Specifically the angular distribution of the photo-fragments momentum. As derived in section 2, the observables can be calculated from the density operator or by using the wavefunctions, equation (6).

From a converged density operator all observables can be calculated. However, individual observables can converged before the full density operators converges. Thus, the numbers of realization for reaching a converged observable is case dependent.

We study the system properties for low intensity and high temperature - $1 \cdot 10^{10} \left[\frac{W}{cm^2} \right], T = 80 [K]$ and high intensity and low temperature- $1 \cdot 10^{13} \left[\frac{W}{cm^2} \right], T = 50 [K]$.

Figure 1 present the angular distribution of the fragments momentum calculated by the direct method, figures 1a-1b, and the RPW method, figures 1c-1d. These results are the outcome of two different intensity of the radiation field, low intensity that can be associated with one-photon transition, figures 1a,1c, and high intensity that represents multi-photons transition, figures 1b,1d. In our previous work [10] we discussed the influence of the laser intensity on the angular distribution of the outgoing momentum. In the present study, we focus on the convergence properties of the random phase wavefunction method.

The angular distribution of the random phase method at low intensity, figure 1c, is comparable to the distribution reached by the exact solution, figure 1a. On the other hand, when comparing the distributions at high intensity, figure 1d to figure 1b, differences are detectable.

The differences between the two methods are compared in figure 1 for both momentum and angu-

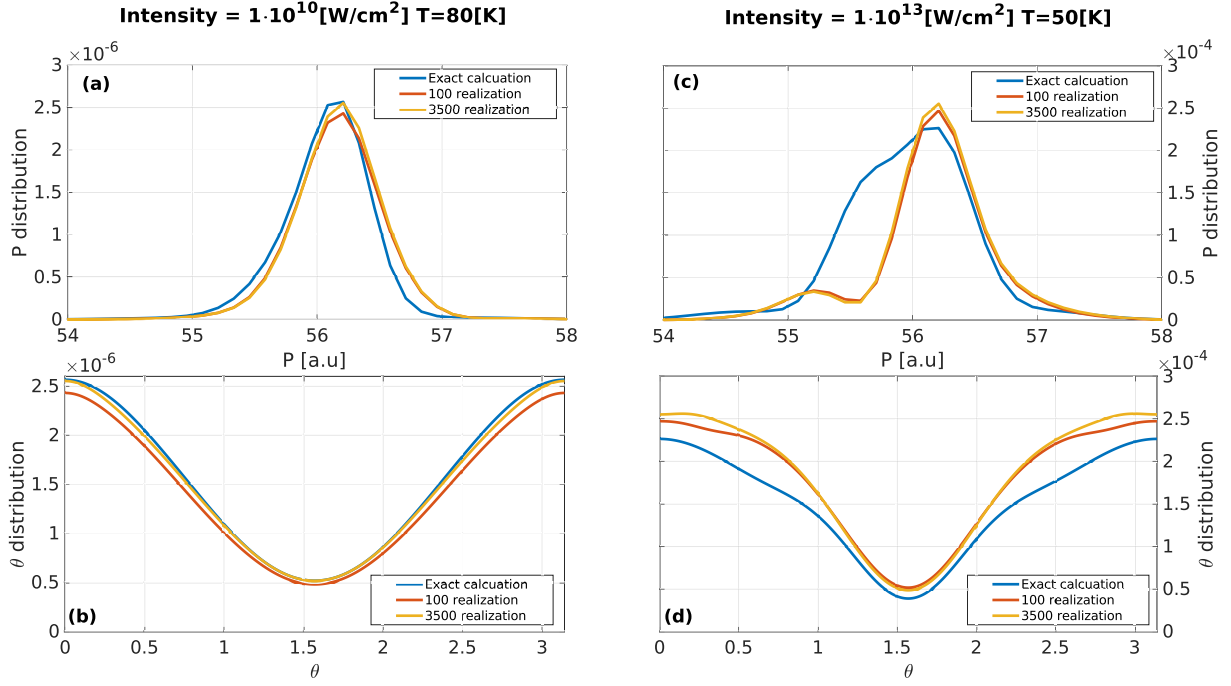


Figure 2: **Upper panel:** The outgoing momentum distribution as a function of the momentum for the exact calculation compared to results obtained with different number of realization. The figure corresponds to low laser intensity, figure2a, and high laser intensity, figure2c. **Lower panel:** The outgoing momentum distribution as a function of the angle θ for the exact calculation and for different realization. Low laser intensity, figure2b, and high laser intensity, figure2d. All the figures correspond to a cut in the corresponding distribution in figure 1.

lar direction. A further analysis is obtained by comparing each direction separately. The upper panel in figure 2 presents the distribution as a function of the momentum, taken at $P_{\perp} = 0$. Note, that only a small range of values from the full momentum grid are plotted. The lower panel at figure 2 presents the distribution as a function of the angle θ , taken at the most probable momentum. At low intensity, the convergence of both distributions to the exact distribution is fast, while at high laser intensity, the distribution has not yet converged to the exact calculation. This discrepancy is the result of significant interference at high intensity. Specifically we see the sensitivity to interference on the momentum and angular distribution.

The convergence properties as a function of the number of realizations is shown in figure 3. First, we show the distance between the distributions as a function of the number of realization calculated by the Wootters metric[16]. We choose to calculate the distance at the momentum distribution, d_W^p , and at the angular distribution, d_W^{θ} , that are computed by equation (11) and equation (12) respectively.

Other properties that we studied are the dissociation probability, \mathcal{P} , and the average kinetic energy, E_k .

The convergence of the distribution is analysed by the distance between the distributions at different laser intensity. By comparing the distance, figures 3a-3b and figures 3e-3f we conclude that the distribution at low intensity, both in angular and momentum, are closer to the exact distributions. Furthermore, in both intensities, the distribution of the momentum is closer to the exact solution than the angular distribution. The distribution distance is sensitive to small differences. In contrast the average kinetic energy is less sensitive as can be view at figure 3c and 3g. The error of the average kinetic energy at both intensities is lower than 1% already after 200 realizations.

The dissociation probability, calculated according to equation (14), at the high intensity increases by orders of magnitude with respect to the low intensity. Therefore, the relative error, that includes division by a very small number, gets a large value and can lead to wrong conclusions. Thus, figures

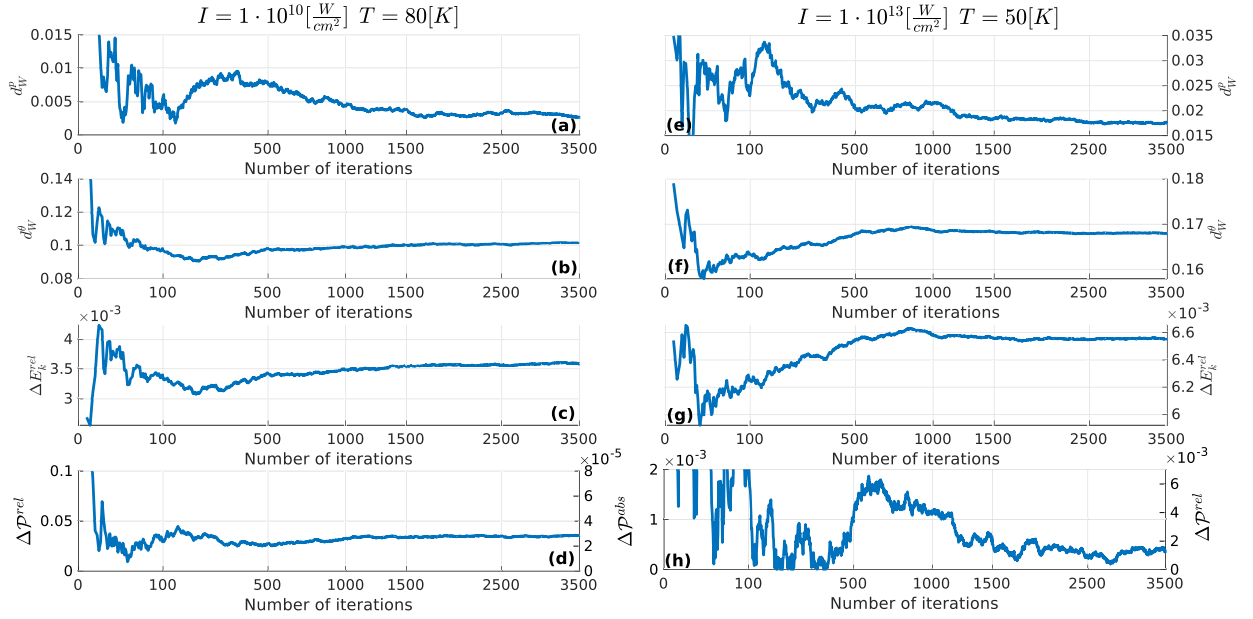


Figure 3: Distributions errors as a function of the number of realization. Results for the low intensity, left panel-figures **a-d**, and high intensity, right panel-figures **e-h**. figures **3a** and **3e**. Displayed is the distance between the momentum distributions comparing the random phase method to the exact calculation, d_W^p , equation 11, while figures **3b** and **3f**, present the distance of the angular distributions, d_W^θ , equation 12. Figures **3c**, **3g** present the relative error in the kinetic energy as a function of the number of realization. Figures **3d**, **3h** shows the error in the dissociation probability, \mathcal{P} . The error is displayed by two axis, the absolute difference between the probabilities, the inner axis. The outer axis display the relative error.

3d and **3h** display the dissociation probability error in two ways: relative error in the outer axis and absolute error in the inner axis. Observing only the relative error can lead to a wrong conclusions that the high intensity calculation gives better results than the low intensity. On the other hand, the absolute error of the high intensity is more significant than at the low intensity.

4 Discussion

An ab-initio simulation method for the strong field photo-dissociation and other time domain spectroscopy is presented. The simulation includes an exact solution of the time-dependent Schrödinger equation. Direct calculation is a complex task, thus the computational complexity scale as N_S^3 , where N_S is the number of state that are involved in the process. The Hilbert space required to describe diatomic photo-dissociation process at typical experimental conditions is vast, of the order 10^6 .

To overcome this challenge of a large Hilbert space, the RPW method has been developed. The initial states is randomly chosen and thermal averaged observables are obtained. The observables are converged to the directly calculated result after a number K of realization, where $K < M_S$. Previous studies on RPA [6, 7, 8] showed that the observable convergence scales as $\sim \frac{1}{\sqrt{K}} \cdot \frac{1}{\sqrt{N_S}}$. In this work, we study the required number of K realizations to converge an observable to the experimental accuracy.

Figure 1 display the angular distribution of the outgoing momentum, which is the significant experimental result. In the figure we present the distribution which is the outcome of the direct calculation and after 3500 RPW realization, for two different radiation intensities. As explain in section 3, those distributions allow to view only a qualitative difference. The distribution can be obtained in each variable separately, angular and momentum, due to the fundamental symmetry of the distribu-

tion. The distributions at each variable, figure 2, provide a visual way to study the convergence, the difference between the RPW after 100 and 3500 realization comparing to the exact calculation.

Figure 2 provide a qualitative comparison between the outgoing momentum distribution for two radiation intensities, figure 2a-2b to figure 2c-2d. At low intensity, the distributions of both direction are converged to the exact calculation, figures 2a-2b, however at high intensity the difference is significant, figure 2c-2d. To quantify the difference between the distributions we use the Wootters distance between them[16]. The distances were calculated between the exact calculated distribution to the distribution after each k realization.

The Wootters metric is a statistical distance between two distribution on the same Hilbert space. Thus the distance can be calculated between the full outgoing momentum distribution or in the angular and momentum direction separately. In this work, we studied the convergence of different observables; thus, we calculated the distance in each direction. The distance between the distribution was normalized to 1 by dividing by $\frac{2}{\pi}$, the maximum value. The distance as a function of the number of realization, for two laser intensities, are presented at figures 3a-3 and figure 3e-f. Each figure presents the convergence for each direction and intensity. Moreover, we concluded, by comparing the four figures, that the distance of the momentum distribution at both intensities starts with lower error and converges faster than the angular distribution.

The outgoing momentum distribution is the most complex observable to converge since it is susceptible to the state of the photo-fragments. Adding a random phase to the initial state leads to a different final state due to interference during the dynamics. At high intensity, where the dynamics is generated by the multi-photons process, the random initial phase leads to very different forms of the final states. This behavior explains the difference in the magnitude of errors; the distance in both directions is shorter at the low intensity than at the high intensity.

The average kinetic energy, ΔE_k^{rel} , is an example of an observable that is less affected by the different interference pathways in the dynamics. The average kinetic energy relative error is presented in figure 3c and figure 3g. The relative error of the two intensities has the same magnitude.

The dissociation probability, \mathcal{P} , is an example of observable in which the different interference, due to the random phase, has a low impact. The probability error is presented in figure 3d and figure 3h. The error is displayed as the absolute and the relative error in the inner and outer axes respectively. The exact probability at low intensity is smaller by four order magnitude from the probability at high intensity. Therefore, one cannot conclude that the error at low intensity is higher than the error at high intensity. The absolute error shows that the dissociation probability, at the two intensities, converges to the exact solution up to the experimental error after only 400 realization.

The observed error leads us to conclude that different observable converge differently. Each observable is sensitive to different properties of the photo-fragments state. The dynamics of the dissociation process includes interferences. Adding random phase changes the interference pattern, leading to different outcome. At high intensity, the process contains multi-photon transition that induces rare events and interferences that lead to a special state. Thus, adding a random phase leads to different events and interference, and so different final state.

In conclusion, we constructed an ab-initio model for time-domain spectroscopy calculating experimental properties. The dynamical processes are computational complex due to the large Hilbert space; we used the RPW method to reduce the complexity. In this study we studied the convergence properties of product observables at two laser intensities. The same method would apply to the dynamical hole left in the reactants [17]. We conclude that the convergence depended on the sensitivity of the observable to the dynamic interferences taking place in the process. Thus, at high laser intensity, where the interference leads to the specific final state, the convergence of sensitive observable is slower.

The presented model is a critical evaluation of random phase computational approaches used to simulate the time-domain spectroscopy in experimental condition. We conclude that depending on the desired experimental outcome the RP method is able to supply accurate observables for realistic

experimental conditions.

Acknowledgements

The author thanks Daniel Strasser, Robert Moszynski, Iwona Majewska, Aviv Aroch. This research was supported by the Israel Science Foundation (Grant No. 510/17).

Appendix

Simulation parameters

The model was set with the parameters from Table 1.

Table 1: Model parameters

parameter	value
μ -reduce mass of F_2^-	9.5 amu
Δr	0.0244 bohr
r_{max}	50 bohr
Temperature	10 K
Initial J_{max} at $T = 10 \text{ K}$	10
J_{max} at high intensity	20
Δt	$5 \cdot 10^{-2} \text{ fsec}$
N_t - number of time steps	7,500
Pulse width	30 fsec
Central wavelength	350 nm
Intensity	$10^{10} \frac{\text{W}}{\text{cm}^2}, 10^{13} \frac{\text{W}}{\text{cm}^2}$
Electronic potentials and dipole momentum	private communication

Theoretical analysis - observables

At the presented work the simulation was set to calculate several observable. This section present detailed equation for each presented observables. As described at section 2 equation 9, the calculation done for each random phase wavefunction and then averaged over K realization. For simplicity we present the observables formula for each random phase wavefunction k , at time the dissociation is over, t_{final} .

The angular distribution of the out going momentum is calculated as follows:

$$\mathcal{D}^k(p, \theta) = \int d\phi \sum_{m, \Omega, n > 0} \left| \sum_j \sum_{\zeta_i} e^{i\chi_{\zeta_i}^k} \sqrt{P_B(j_i)} \sqrt{a_{n,0,\zeta,\zeta_i}(t = t_{final})} \cdot D_{m,\Omega}^j(\theta, \phi) \right|^2 \quad (10)$$

Note, the summation over j is quantum summation that conserve phases while the summation over m and Ω are classical. The different is outcome of the dynamic, which only generate coherence between different values of j with the same values of m and Ω .

The distance between the outcome distribution after K realization to the exact distribution is calculated by the Wootters metric as follows:

$$d_W^p(K) = \frac{\pi}{2} \cos^{-1} \left(\int dp \sqrt{\mathcal{D}_{rand}^K(p, \theta = 0)} \cdot \sqrt{\mathcal{D}_{exact}^K(p, \theta = 0)} \right) \quad (11)$$

$$d_W^\theta(K) = \frac{\pi}{2\pi} \cos^{-1} \left(\int d\theta \sqrt{\mathcal{D}_{rand}^K(p = p_{mp}, \theta)} \cdot \sqrt{\mathcal{D}_{exact}^K(p = p_{mp}, \theta)} \right) \quad (12)$$

We choose to calculate the distribution at the momentum direction, d_W^p , and the angular direction separately, d_W^θ . For each calculation we set one of the direction at the most probable value, $\theta = 0$ and $p = p_{mp}$.

The dissociation probability and the kinetic energy are calculated from the final wavefunction as follows:

$$\mathcal{P}^k = \left\langle \Psi_{n \neq 0}^k(r, \theta, \varphi; t = t_{final}) \mid \Psi_{n \neq 0}^k(r, \theta, \varphi; t = t_{final}) \right\rangle \quad (13)$$

$$\mathcal{E}_k = \left\langle \Psi_{n \neq 0}^k(r, \theta, \varphi; t = t_{final}) \mid \hat{P}^2 \mid \Psi_{n \neq 0}^k(r, \theta, \varphi; t = t_{final}) \right\rangle \quad (14)$$

References

- [1] Max Born and Robert Oppenheimer. “Zur quantentheorie der molekeln”. In: *Annalen der physik* 389.20 (1927), pp. 457–484.
- [2] Luiz Guilherme Machado de Macedo et al. “Relativistic four-component MRCISD+ Q calculations of the six lowest valence states of molecular F_2^- anion including Breit interactions”. In: *Journal of Molecular Modeling* 27.8 (2021), pp. 1–8.
- [3] Iwona Majewska Robert Moszynski. “Private Communication”. In: . (2019).
- [4] Abhishek Shahi, Yishai Albeck, and Daniel Strasser. “Intense-Field Multiple-Detachment of F_2^- : Competition with Photodissociation”. In: *The Journal of Physical Chemistry A* 121.16 (2017), pp. 3037–3044.
- [5] Abhishek Shahi, Yishai Albeck, and Daniel Strasser. “Ultrafast F_2^- photodissociation by intense laser pulses: a time-resolved fragment imaging study”. In: *EPJ Web Conf.* Vol. 205. EDP Sciences. 2019, p. 09012.
- [6] David Gelman and Ronnie Kosloff. “Simulating dissipative phenomena with a random phase thermal wavefunctions, high temperature application of the Surrogate Hamiltonian approach”. In: *Chemical physics letters* 381.1-2 (2003), pp. 129–138.
- [7] Shimshon Kallush and Sharly Fleischer. “Orientation dynamics of asymmetric rotors using random phase wave functions”. In: *Physical Review A* 91.6 (2015), p. 063420.
- [8] Jin-Wei Hu and Yong-Chang Han. “Investigation of photoassociation with full-dimensional thermal-random-phase wavefunctions”. In: *The Journal of Chemical Physics* 155.6 (2021), p. 064108.
- [9] Jin-Wei Hu and Yong-Chang Han. “The thermal-average effect on the field-free orientation of the NaI molecule with full-dimensional random-phase wavefunctions”. In: *Chemical Physics Letters* 783 (2021), p. 139052. ISSN: 0009-2614.
- [10] Bar Ezra, Shimshon Kallush, and Ronnie Kosloff. “Dissociation in strong field: A quantum analysis of the relation between angular momentum and angular distribution of fragments”. In: *Chemical Physics Letters* 756 (2020), p. 137845.
- [11] Richard N.. Zare. *Angular momentum: understanding spatial aspects in chemistry and physics*. J. Wiley & Sons, 1988.

- [12] Hillel Tal-Ezer and Ronnie Kosloff. “An accurate and efficient scheme for propagating the time dependent Schrödinger equation”. In: *The Journal of chemical physics* 81.9 (1984), pp. 3967–3971.
- [13] Ronnie Kosloff. “Propagation methods for quantum molecular dynamics”. In: *Annual review of physical chemistry* 45.1 (1994), pp. 145–178.
- [14] Rongqing Chen and Hua Guo. “The Chebyshev propagator for quantum systems”. In: *Computer physics communications* 119.1 (1999), pp. 19–31.
- [15] Ran Damari, Shimshon Kallush, and Sharly Fleischer. “Rotational control of asymmetric molecules: dipole-versus polarizability-driven rotational dynamics”. In: *Physical review letters* 117.10 (2016), p. 103001.
- [16] William K Wootters. “Statistical distance and Hilbert space”. In: *Physical Review D* 23.2 (1981), p. 357.
- [17] Uri Banin et al. “Impulsive excitation of coherent vibrational motion ground surface dynamics induced by intense short pulses”. In: *The Journal of chemical physics* 101.10 (1994), pp. 8461–8481.